Proc. Natl. Acad. Sci. USA
Vol. 76, No. 3, pp, 1228–1232, March 1979
Biophysics

Dark field imaging of biological macromolecules with the scanning transmission electron microscope

(phase contrast/low-dose electron microscopy/unstained biological macromolecules/dark field contrast/thin carbon films)

MITSUO OHTSUKI*, MICHAEL S. ISAACSON*†, AND A. V. CREWE*†‡

*Enrico Fermi Institute, and †Department of Physics, and ‡Department of Biophysics and Theoretical Biology, The University of Chicago, Chicago, Illinois 60637

Contributed by Albert V. Crewe, December 21, 1978

ABSTRACT **A scanning transmission electron microscope (STEM) equipped with a field emission gun has been employed for the examination of biological macromolecules at high resolution. The quality of micrographs obtained with the STEM is dependent upon the quality of the substrate used to support biological objects because the image contrast in dark field is proportional to the mass density of the specimen. In order to reduce deleterious effects of the substrates on the image quality, we have developed a method of fabricating substrates consisting of very thin, very clean carbon films supported on very clean fenestrated plastic films. These films are approximately 15 Å thick. Well-known biological macromolecules such as glutamine synthetase and tobacco mosaic virus (both stained) and low-density lipoprotein and ferritin (both unstained) were placed on these substrates and examined with the STEM by using various modes of contrast. The micrographs obtained by using the dark field mode of contrast employing an annular detector were free from phase contrast, as expected. Using this contrast mode, we have been able to directly observe (in-focus) 2.5- to 4.4-Å lattice spacings in the ferritin core. The effect of electron radiation damage on the helical structure of tobacco mosaic virus was also examined. Micrographs as well as corresponding optical diffraction patterns obtained with moderately low doses showed very clear helical structure from both sides of the virus. In addition, the (11.5 Å)$^{-1}$ layer lines indicated the effective resolution attained on these particles.**

In a scanning transmission electron microscope (STEM), a high-resolution image can be formed by scanning an electron beam (which can be less than 3 Å in diameter) across a specimen in a raster fashion while collecting the transmitted elastically scattered electrons with an annular detector located beneath the specimen (1). The electron current striking this detector is then used to modulate the intensity of a synchronously scanned display (usually in the form of a cathode ray tube or a television). Under appropriate conditions, the fraction of the incident electron beam that scatters and strikes this detector is approximately proportional to $M_A Z^{3/2}$, in which M_A is the mass per unit area of the specimen for the region that the beam has passed through and Z is the average atomic number. Images formed by using the signal from this detector are virtually free of phase contrast artifacts and represent the true projected mass density of the specimen (2, 3). In addition to giving this signal (which we call the elastic dark field signal), the transmitted electrons that pass through the hole in the annular detector can be analyzed as to whether or not they have lost energy. Images can then be formed by using those energy loss electrons (the inelastic dark field signal) or the no-loss electrons (the filtered bright field signal). The advantage of using such dark field signals is that not only do they represent the mass density of the specimen (one can, in fact, measure mass by using these signals), but also the efficiency of collection can be as high as 80% (4, 5).

The publication costs of this article were defrayed in part by page charge payment. This article must therefore be hereby marked "*advertisement*" in accordance with 18 U. S. C. §1734 solely to indicate this fact.

Because radiation damage is a limitation in biological microscopy (see, e.g., refs. 6 and 7) this efficiency is of importance in obtaining images by using a minimal dose of electrons. Furthermore, because beam scanning and deflection coils are an inherent part of the STEM, one automatically has the ability to focus on one area and record a micrograph from the adjacent area.

It is the purpose of this paper to demonstrate the utility of the STEM for observing biological structures at high resolution.

MATERIALS AND METHODS

Supporting Film. The supporting film is important because the quality of the film may alter the image of the micrographs obtained in the STEM. In our experiments, spectroscopic grade graphite rods (Union Carbide) were used to evaporate carbon onto either cleaved NaCl crystals or mica in a conventional evaporator (Varian E-10) (8). This evaporator has a liquid nitrogen cold trap between the vacuum chamber and the diffusion pump. Regular grade carbon rods were not suitable because these contain heavy atom contaminants (3). All parts for the evaporation inside the bell jar were replaced with ones made of stainless steel, which were cleaned initially with 20% HNO_3, then acetone, and then ethyl alcohol. The cleaning was performed to eliminate any possible organic contamination. The thickness of the carbon support films was determined by measuring the amount of inelastic scattering of electrons from the film (2, 3). Fig. 1 shows typical very thin carbon films used for our experiments. (Fig. 1*a*) average thickness of 14 Å deposited on a NaCl substrate and (Fig. 1*b*) average thickness of 16 Å deposited on a mica substrate. More than 95% of the open area is covered by the film. We have found no apparent difference in the film quality made with either the NaCl or the mica substrate.

Fenestrated Films (Microgrids). High-quality fenestrated support films are essential for supporting the very thin carbon films necessary for high-resolution scanning transmission microscopy. In biological specimen preparation, good coverage of the grid is an important practical requirement (see Fig. 1 *c*). Thus holes in the fenestrated film must occupy at least 75% of the area. We employed a modified (8) Fukami–Adachi method (9) that fulfills this requirement without any trace of heavy atom contamination on the substrate. The fenestrated films were placed on titanium grids (75 × 300 mesh; Ernest Fullam, Schenectady, NY) because: (*i*) titanium can be cleaned (20% HNO_3) prior to acetone and ethyl alcohol cleaning, (*ii*) it has a low atomic number, Z = 22, and (*iii*) it has a much lower solubility in H_2O than copper does. Effects from possible contamination at the atomic level from heavy metals can thus be minimized. Thick carbon (≈1500 Å) was then evaporated as

Abbreviations: STEM, scanning transmission electron microscope; CTEM, conventional transmission electron microscope; TMV, tobacco mosaic virus; e, electron.

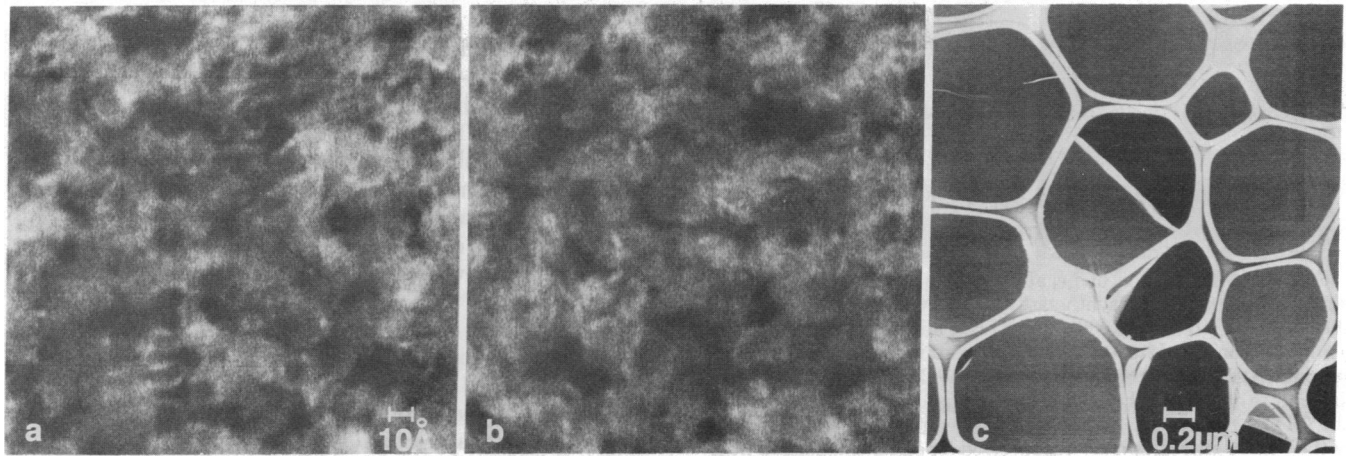

FIG. 1. Very thin carbon films made on NaCl (*a*) and mica (*b*), shown at high magnification (×3,250,000). The average thicknesses of the films were 14 Å (*a*) and 16 Å (*b*). These films were used for biological specimen preparation. The resolution of these STEM micrographs is better than 3 Å. The films were free from heavy atom contamination. (*c*) Very thin carbon film covering fenestrated film. (×20,000.)

a backing on the side of the grid facing the fenestrated film. An additional 500 Å thickness of carbon was evaporated onto the other side of the grid to prevent possible charging and also to prevent contamination onto the sample from the plastic support.

Decontamination of the Grid. One of the important problems in the preparation of specimens for the STEM is the necessity of using very clean techniques to minimize both heavy atom and hydrocarbon contamination. We found that when the supporting grid was very clean, contamination problems were minimized. Prior to deposition of the sample, the grids with the thin carbon film supported by the fenestrated film (microgrid) were decontaminated by heating them in the air with a 100-W lamp from a distance of 5 cm for 10 min. This procedure results in no detectable contamination after illumination of areas as small as 232 × 232 Å with doses in excess of 10^7 electrons (e)/Å^2.

Specimen Preparation for Electron Microscopy. All samples were placed on very thin carbon films as described above: (*i*) For glutamine synthetase, the samples were diluted to 100 μg/ml with distilled water. The molecules were then negatively stained with 1% sodium phosphotungstate (pH 7.0) or 1% uranyl formate and then dried in air. In some cases, the specimens were dried by critical point drying after being stained with 1% uranyl formate in an ethyl alcohol solution. Some specimens were fixed prior to staining with 1% OsO_4, 1% glutaraldehyde, or both for 2 min. (*ii*) Tobacco mosaic virus (TMV) intact particles were diluted to 400 μg/ml with distilled water. Uranyl acetate (1%) was applied for negative staining. The specimens were then air-dried. (*iii*) The samples of low-density lipoprotein were diluted to 100 μg/ml with 10 mM NH_4HCO_3 buffer (pH 8.0). The unstained samples were either air-dried or freeze-dried. (*iv*) For ferritin, the particles were diluted to 350 μg/ml with distilled water, then deposited on the carbon substrate and air-dried.

Electron Microscopy. *Scanning transmission electron microscopy.* The STEM was operated at an accelerating voltage of 37.3 kV. Micrographs were recorded on 35-mm Kodak Tri-X film (ASA 400) from the display oscilloscope, which is capable of recording 1024 × 1024 picture elements. A square of 232 Å, 705 Å, or 2250 Å was scanned to form the image. Both elastic and inelastic signals were employed for the experiments (see *Results and Discussion*). In all the experiments, the inner half angle subtended by the annular detector was greater than or equal to twice the beam convergence half angle (which was 0.015 rad). Micrographs taken with this detector geometry are relatively free from phase contrast effects (2, 5). Optical diffraction was employed for analyzing the low-dose micrographs. A Kodak Super-XX pan film 4142 (ASA 200) was used for the recording.

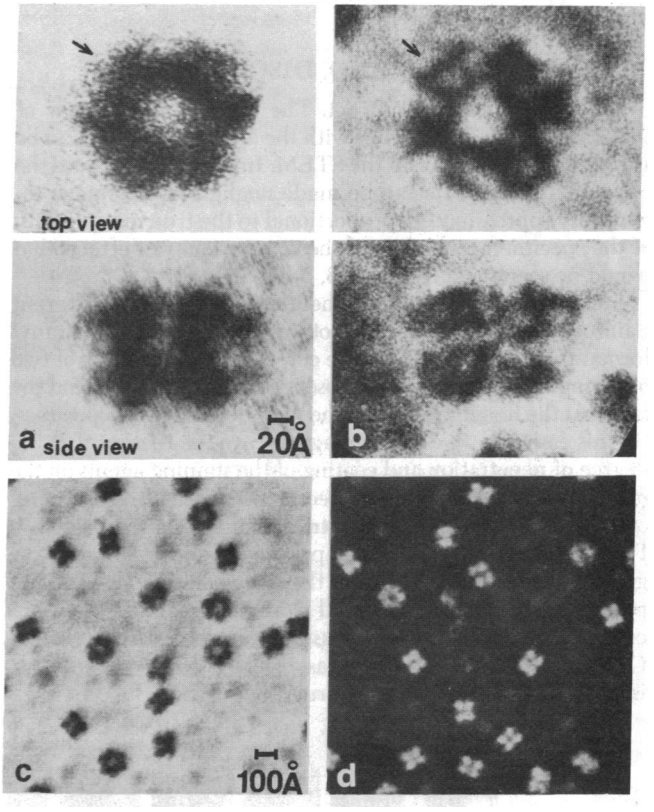

FIG. 2. STEM micrographs of negatively stained glutamine synthetase from *Anabaena* 7120 (a blue-green alga). One percent sodium phosphotungstate (*a*) and 1% uranyl formate (*b*) were used for comparison of the penetration of these staining agents. The molecule consists of a double disk of two opposing hexamers. The top and side views are shown. The difference of the penetration of the staining agent is very obvious (see arrows). These micrographs at high magnification (×1,500,000) are taken with elastic signal (I_{el}), and are free of phase contrast effects. (*c* and *d*) A dark field image (*c*) from the elastic signal (I_{el}) and a bright field image (*d*) from the unscattered signal (I_u) are shown at low magnification (×270,000). One percent sodium phosphotungstate was used for the negative staining and the specimens were air-dried. The sample was made and kindly provided by James Orr and Robert Haselkorn of the University of Chicago.

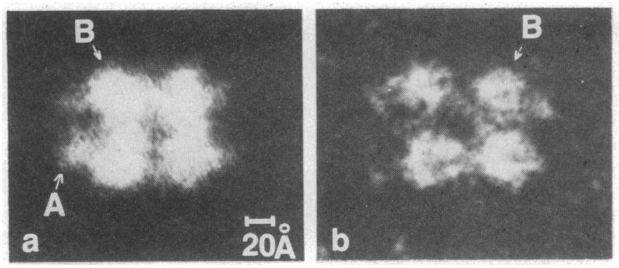

FIG. 3. Micrographs of negatively stained (1% sodium phosphotungstate) glutamine synthetase obtained with the STEM (*a*) and the CTEM (*b*). (×1,5000,000). The STEM micrograph (obtained by using the annular detector signal) (*a*) permits us to see the single subunit (A) as well as the superimposed one (B). Single subunits are difficult to observe in the CTEM micrograph (*b*). The fine details in the CTEM micrograph arise from phase contrast effects. Contrast of the STEM micrograph (*a*) was reversed for easier comparison with the CTEM micrograph (*b*). The sample was dried in air.

Conventional transmission electron microscopy. Some negatively stained specimens were examined with a Hitachi HU-11A conventional transmission electron microscope (CTEM) for image comparison with the STEM micrographs. The CTEM in micrographs were taken with 75-kV electrons at an electron optical magnification of ×42,000 using an objective aperture half angle of 0.014 rad. The defocus (Δf) was kept at approximately −1000 Å to obtain maximum resolution with phase contrast (10, 11).

RESULTS AND DISCUSSION

Absence of Phase Contrast. The collection efficiency of elastically scattered electrons with the annular detector can be as high as 80% or more in the STEM. In addition, because the phase contrast effects can be made negligible, the image intensity is approximately proportional to the true mass density of the specimen with none of the reverse contrast effects that would be seen in a CTEM (2, 3, 5, 10–12).

Fig. 2 shows glutamine synthetase stained by two different staining agents, sodium phosphotungstate (Fig. 2*a*) and uranyl formate (Fig. 2*b*). The molecule consists of a double disk of two opposing hexamers. Both the absence of phase contrast and the fact that the image represents the mass density of the specimen (in this case negative staining agents) are the reasons that the degree of penetration and coating of the staining agents on the macromolecules can be detected very easily. We can clearly observe the difference of penetration of the staining agent in Fig. 2, where uranyl formate appears to have penetrated to a greater degree into subunits of the molecules than has sodium phosphotungstate. Fig. 2 *c* and *d* are low-magnification micrographs of the phosphotungstate-stained particles. In the CTEM, because of phase contrast effects, these same comparisons at such high resolutions are rather difficult.

The advantage of the STEM over the CTEM, particularly at high resolution, can be seen by comparing two sodium phosphotungstate-stained identical particles as seen in Fig. 3, where we show the negatively stained glutamine synthetase taken with the STEM and the CTEM. Fine details seen in the CTEM micrograph are from phase contrast effects that can be misinterpreted. In addition, because of the high collection efficiency of electrons, a single subunit (A) as well as superimposed subunit (B) can be observed in the STEM. In the CTEM micrograph, however, it is only possible to see the superimposed subunits (B).

In the CTEM, micrographs have to be taken at specific conditions of defocus in order to obtain maximum resolution (10). In the STEM, however, the highest resolution is obtained in-focus (i.e., when the beam has its minimum diameter). Uranyl acetate-stained particles of TMV were examined with a through focal series as seen in Fig. 4. The in-focus micrograph (Fig. 4*c*) corresponds to the highest resolution in which both phase contrast and diffraction contrast are obviously absent.

Low-Dose Electron Microscopy. One of the advantages of using the STEM is that we can accurately control the electron dose (3, 6) by changing either the magnification or the beam current. The change of magnification from M_1 to M_2 changes the number of electrons per unit area hitting the specimen as the ratio $(M_1/M_2)^2$ because a fixed number of electrons scans a given area of the specimen if the beam current is constant. In addition, the dose can be precisely controlled by changing the field of view with the beam deflection coils. In our system, we can consecutively scan 48 different fields of view after setting the focus at the beginning of the sequence. To change the beam current, one merely changes the emission current from the electron gun. Low-dose experiments in the CTEM are generally carried out by procedures that involve a change of electron optics (e.g., the setting of the second condenser lens), or mechanical motion (e.g., lens pole pieces or specimen stage), or both (13–15). These methods are rather complicated compared to that of the STEM system, in which neither a change of electron optics nor mechanical motions are involved. A micrograph of the field of view not previously exposed to electrons can be obtained by using the montage sequence as noted above. In addition, with the STEM one can precisely measure the electron dose hitting the viewing area because the detector signal is proportional to the number of electrons striking it.

One of the effects of beam dose on image quality was illustrated by using negatively stained particles of TMV. TMV has a helical repeat of 23 Å and 16⅓ subunits per turn (16). The diffraction pattern from the low-dose (11 e/Å^2) micrograph clearly shows a pair of spots corresponding to both sides of the helical repeat of 23 Å (see arrows in Fig. 5*a*). These two diffraction spots from both sides of the helical repeat of intact virus of TMV have not previously been seen by electron microscopy.

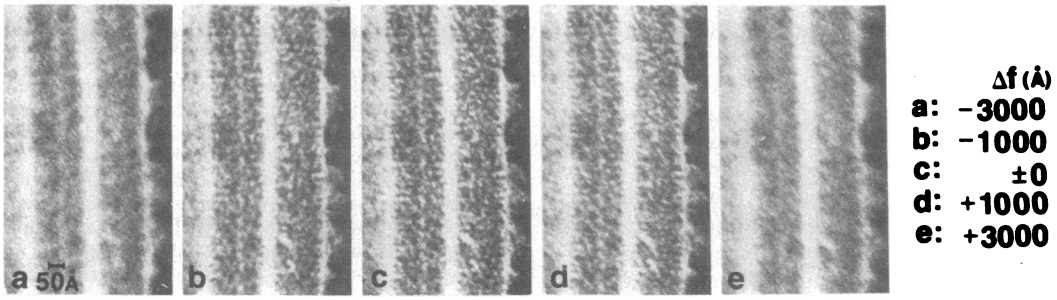

FIG. 4. STEM micrographs of negatively stained (1% uranyl acetate) TMV were examined with a through-focal series at high resolution. (×430,000.) The highest resolution can be obtained when the micrograph is taken in-focus ($\Delta f = 0$; see *c*). There are neither phase contrast nor diffraction contrast effects seen in the STEM micrograph taken with the annular detector elastic signal (I_{el}). The sample was kindly provided by Milton P. Gordon of the University of Washington, Seattle, WA. Δf, Defocus value.

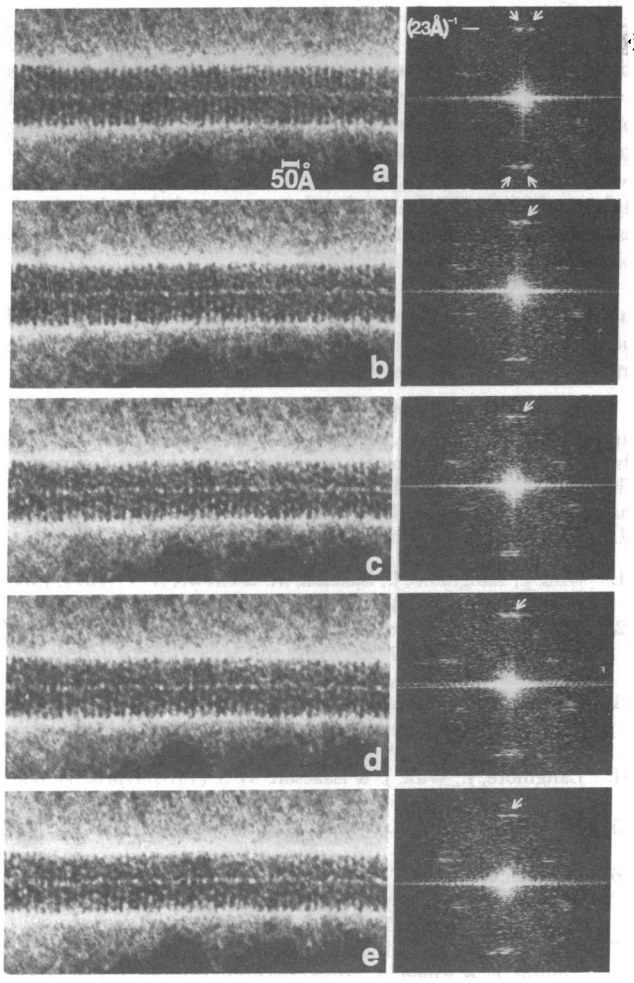

FIG. 5. Low-dose STEM micrographs (*Left*) (×470,000) (obtained by using the annular detector signal) and the corresponding optical diffraction patterns (*Right*) of negatively stained (1% uranyl acetate) TMV. The electron doses were: *a*, 11 e/Å^2; *b*, 22 e/Å^2; *c*, 33 e/Å^2; *d*, 44 e/Å^2; *e*, 66 e/Å^2. The effects of electron radiation damage can be observed by comparing the helical structure. The pair of diffraction spots corresponding to both sides of the helical repeat of 23 Å (see arrows) is smeared out to a single spot as the dose increases.

Some authors have shown optical diffraction patterns in conjunction with electron micrographs of TMV, but the corresponding diffraction spots from both sides of the particles were smeared out into single spots, presumably due to damage by electron irradiation (17). Effects of the radiation damage can easily be seen by observing that these spots smear out to a single spot and the intensity decreases as the electron dose increases, as seen in Fig. 5: *b*, 22 e/Å^2; *c*, 33 e/Å^2; *d*, 44 eÅ^2; *e*, 66 e/Å^2. In addition, the micrographs shown along with their corresponding optical diffraction patterns indicate that the staining agent had coated and embedded evenly the TMV molecules. An additional low-dose (11 e/Å^2) in-focus STEM micrograph is shown in Fig. 6*a*). In Fig. 6*b* and *b'*, we show optical diffraction patterns from the portion A of the micrograph shown in Fig. 6*a* in which the (11.5 Å)$^{-1}$ layer lines (though weak) can be seen.

Observation of Unstained Biological Specimens. Unlike negatively stained biological molecules, an unstained biological object is difficult to observe in the CTEM, even when dark field techniques are used. In the STEM, however, observation is much easier because the collection efficiency for elastically scattered electrons can be more than 10 times higher than in the CTEM. Fig. 7 shows a micrograph of an unstained low-density lipoprotein taken using the elastic annular detector

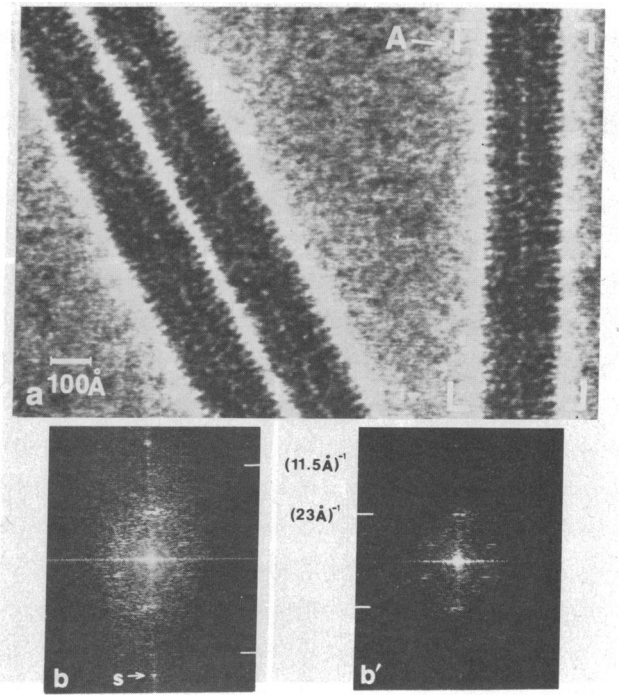

FIG. 6. (*a*) Low-dose (11 e/Å^2) STEM micrograph of negatively stained (1% uranyl acetate) TMV at high magnification (×533,000). (*b* and *b'*) Optical diffraction patterns from the portion A of the micrograph (*a*). The (11.5 Å)$^{-1}$ layer lines can be seen. *b* and *b'* were from the same negative and printed in such a manner that both the high and lower spatial frequency regions can be observed. s corresponds to diffraction spots due to every fourth scan line.

signal. The contrast of unstained molecules can be as high as that of stained ones, as seen in this figure. The effective resolution on the particle is better than 10 Å in this micrograph, which was recorded with an electron dose of 19 e/Å^2. The carbon film used in this preparation was a 16 Å thin film deposited on mica.

Another advantage of the STEM is that one can observe images with various combinations of signals (2, 3). Unstained ferritin particles from horse spleen were employed to demonstrate the use of such signals. Ferritin consists of protein in its outer shell and iron in the inner core. The iron cores have substructures that are believed to be crystalline (18). Because the elastic signal (I_{el}) and the inelastic signal (I_{in}) can be written (2) as $I_{el} \propto Z^{3/2}$, $I_{in} \propto Z^{1/2}$, we can form an image from a signal, $I_{in} - CI_{el}$, in which the elastic signal is first multiplied by the constant C and then subtracted from the inelastic signal. C can then be chosen to emphasize a particular Z. For instance, when we want to visualize the iron core within the protein shell, we set C to obtain $I_{in} - CI_{el} \simeq 0$ for iron. Thus, the iron core will

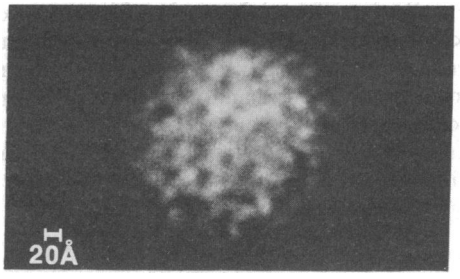

FIG. 7. Low-dose (19 e/Å^2) STEM micrograph of freeze-dried unstained low-density lipoprotein. (×2,000,000.) Note the high contrast, in which the effective resolution on the particle is better than 10 Å. The sample was kindly provided by Angelo M. Scanu of the University of Chicago.

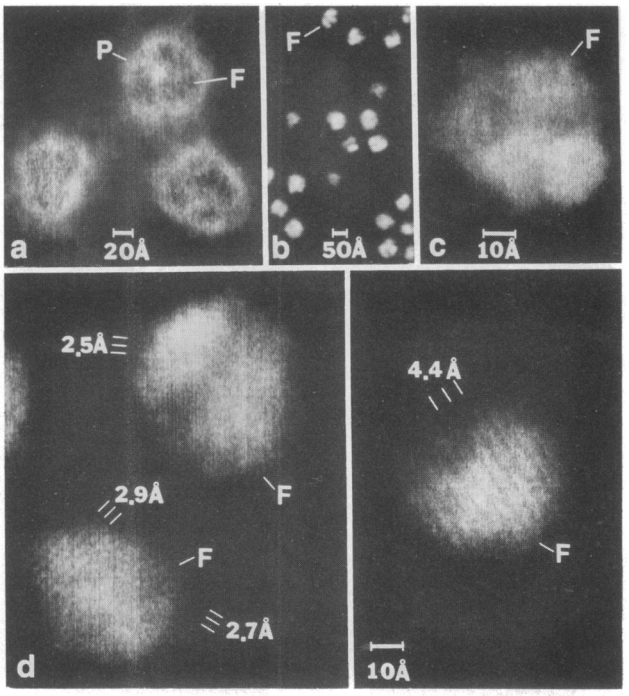

FIG. 8. STEM micrograph of unstained ferritin molecules from horse spleen (Sigma). (*a*) Image formed by a subtraction signal ($I_{in} - CI_{el}$) at high magnification (×1,400,000). Iron cores F can be seen as dark contrast while the protein shells P appear light. (*b–d*) Micrographs obtained by using the elastic signal (I_{el}) only (*b*, ×430,000; *c* and *d*, ×4,180,000). Only the iron cores can be observed. The presence of the substructure is apparent. Crystalline lattices of 2.5- to 4.4-Å spacings can be seen in *d*.

appear dark while the protein shell appears light (19). In this procedure, both shell and core can be thus imaged without losing information about either one as seen in Fig. 8*a*. Fig. 8*b–d* shows only iron cores of ferritin, taken by using the elastic signal. Substructures of the iron core are clearly seen in these micrographs, in which some of the substructures show lattices of 2.5–4.4 Å. These observations are consistent with those of Massover and Cowley (18), who used diffraction contrast in the CTEM. Because both phase contrast and diffraction contrast effects are absent with appropriate annular detector geometry, we expect to see such domains only when the crystalline planes are exactly parallel to the incident beam.

CONCLUSION

The quality of the grids plays a very important role in high-resolution scanning transmission electron microscopy if one wants to visualize unstained biological specimens or heavier single atoms. We have found that carbon films approximately 15 Å thick, which are free from heavier atom contamination, can be prepared by using a conventional evaporator. These films are reasonably uniform and relatively sturdy, and more than 95% of the open area is covered by the film. Thus they are quite useful as supports for biological specimens (both stained and unstained).

By placing various biological macromolecules on these substrates, we have shown several advantages of the STEM. The absence of both phase contrast and diffraction contrast effects gives artifact-free micrographs. Stained as well as unstained specimens can be efficiently visualized, image intensity being approximately proportional to mass density. In addition, controlled electron dose experiments can be easily carried out at high resolution. We have also demonstrated that the visualization of specimens with combined signals can be very useful for high-resolution observation.

The STEM, which has many advantages over the CTEM, should thus play an important role for the structural studies of biological specimens at high resolution for which both low dose and true contrast are definitely required.

We thank Prof. R. Haselkorn and Dr. J. Orr for providing us glutamine synthetase, and Prof. M. P. Gordon for providing us TMV. We also thank Prof. A. M. Scanu for providing us low-density lipoprotein. This work was supported by the Biotechnology Resources Branch of the National Institutes of Health, and the U.S. Department of Energy. M.S.I. was an Alfred P. Sloan Faculty Fellow.

1. Wall, J., Langmore, J., Isaacson, M. & Crewe, A. V. (1974) *Proc. Natl. Acad. Sci. USA* **71**, 1–5.
2. Crewe, A. V., Langmore, J. & Isaacson, M. S. (1975) in *Physical Aspects of Electron Microscopy and Microbeam Analysis*, eds. Siegel, B. & Beaman, D. (Wiley, New York), pp. 47–62.
3. Isaacson, M. S., Langmore, J. & Wall, J. (1974) in *Proceedings of Scanning Electron Microscopy/1974*, eds. Johari, O. & Corvin, I. (IITRI, Chicago), Vol. 1, pp. 19–26.
4. Langmore, J., Wall, J. & Isaacson, M. S. (1973) *Optik* **38**, 335–350.
5. Wall, J., Isaacson, M. S. & Langmore, J. (1974) *Optik* **39**, 353–374.
6. Isaacson, M. S. (1977) in *Principle and Techniques of Electron Microscopy*, ed. Hayat, M. A. (Van Nostrand-Reinhold, New York), Vol. 7, pp. 1–78.
7. Ottensmeyer, F. P., Bazett-Jones, D. P., Rust, H. P., Weiss, K., Zemlin, F. & Engel, A. (1978) *Ultramicroscopy* **3**, 191–202.
8. Ohtsuki, M., Isaacson, M. S. & Crewe, A. V. (1979) *Scanning Electron Microscopy/1979*, ed. Johari, O. (SEM, Inc., Chicago), in press.
9. Fukami, A. & Adachi, K. (1965) *J. Electron Microsc.* **14**, 112–118.
10. Johnson, D. J. & Crawford, D. (1973) *J. Microsc. (Oxford)* **98**, 313–324.
11. Ohtsuki, M. & Sogard, M. (1978) *Proceedings Ninth International Congress on Electron Microscopy, Toronto, Canada*, ed. Sturgess, J. (Microscopy Society of Canada, Toronto), Vol. 2, pp. 170–171.
12. Engel, A., Dobochet, J. & Kellenberger, E. (1976) *J. Ultrastruct. Res.* **57**, 322–330.
13. Unwin, P. N. T. (1974) *J. Mol. Biol.* **87**, 657–670.
14. Williams, R. C. & Fisher, H. W. (1970) *J. Mol. Biol.* **52**, 121–123.
15. Unwin, P. N. T. & Henderson, R. (1974) *J. Mol. Biol.* **94**, 245–440.
16. Franklin, R. E. & Holmes, K. C. (1958) *Acta Crystallogr.* **11**, 213–220.
17. Klug, A. & DeRosier, D. J. (1966) *Nature (London)* **212**, 29–32.
18. Massover, W. H. & Cowley, J. M. (1973) *Proc. Natl. Acad. Sci. USA* **70**, 3847–3851.
19. Isaacson, M. S. (1976) *Proceedings of the Sixth European Congress on Electron Microscopy, Jerusalem*, ed. Brandon, D. G. (TAL International, Israel), Vol. 1, pp. 26–30.